The EMBO Journal (2013) 32, 954–969
www.embojournal.org

SOURCE DATA | TRANSPARENT PROCESS

THE EMBO JOURNAL

Bassoon and Piccolo maintain synapse integrity by regulating protein ubiquitination and degradation

Clarissa L Waites[1,2,*], Sergio A Leal-Ortiz[1], Nathan Okerlund[1], Hannah Dalke[2], Anna Fejtova[3], Wilko D Altrock[3], Eckart D Gundelfinger[3] and Craig C Garner[1,*]

[1]Nancy Pritzker Laboratory, Department of Psychiatry and Behavioral Sciences, Stanford University School of Medicine, Palo Alto, CA, USA, [2]Departments of Pathology and Cell Biology and Neuroscience, Columbia University Medical Center, New York, NY, USA and [3]Department of Neurochemistry and Molecular Biology, Leibniz Institute for Neurobiology, Magdeburg, Germany

The presynaptic active zone (AZ) is a specialized microdomain designed for the efficient and repetitive release of neurotransmitter. Bassoon and Piccolo are two high molecular weight components of the AZ, with hypothesized roles in its assembly and structural maintenance. However, glutamatergic synapses lacking either protein exhibit relatively minor defects, presumably due to their significant functional redundancy. In the present study, we have used interference RNAs to eliminate both proteins from glutamatergic synapses, and find that they are essential for maintaining synaptic integrity. Loss of Bassoon and Piccolo leads to the aberrant degradation of multiple presynaptic proteins, culminating in synapse degeneration. This phenotype is mediated in part by the E3 ubiquitin ligase Siah1, an interacting partner of Bassoon and Piccolo whose activity is negatively regulated by their conserved zinc finger domains. Our findings demonstrate a novel role for Bassoon and Piccolo as critical regulators of presynaptic ubiquitination and proteostasis.

The EMBO Journal (2013) **32,** 954–969. doi:10.1038/emboj.2013.27; Published online 12 February 2013
Subject Categories: proteins; neuroscience
Keywords: active zone; Bassoon; Piccolo; Siah1; ubiquitination

Introduction

Presynaptic boutons release chemical neurotransmitter at specialized sites called 'active zones' (AZs) (Schoch and Gundelfinger, 2006). Ultrastructurally, AZs are defined by geometric arrays of electron-dense material that extend 50–200 nm inward from the plasma membrane to the synaptic vesicle (SV) pool (Harlow *et al*, 2001; Siksou *et al*, 2007). This material, the cytoskeletal matrix assembled at the AZ (CAZ), is comprised of multidomain scaffold proteins including RIMs, Munc13, Liprin1α, ELKS/CAST, Bassoon, and Piccolo (Fejtova and Gundelfinger, 2006; Jin and Garner, 2008). These molecules are hypothesized to function both as structural organizers of the AZ and as regulators of SV exocytosis. However, while the roles of some of these (i.e., RIMs and Munc13) are well documented, others remain poorly understood (Fejtova and Gundelfinger, 2006; Jin and Garner, 2008).

The two largest CAZ proteins, Piccolo and Bassoon, are particularly enigmatic due to their vertebrate-specific expression and highly complex gene structures, which have hampered efforts to create adequate genetic knockout models (Waites *et al*, 2011). Both are expressed during neuronal differentiation (Cases-Langhoff *et al*, 1996; Zhai *et al*, 2000) and are among the first proteins to arrive at nascent synapses (Friedman *et al*, 2000; Zhai *et al*, 2000; Shapira *et al*, 2003), implicating them in synapse formation (Ziv and Garner, 2004; Waites *et al*, 2005). In addition, mice lacking a central domain of Bassoon exhibit major structural defects in ribbon synapses of the retina and cochlea, including aberrant clustering of voltage-gated calcium channels and dissociation of ribbons from the presynaptic membrane (Altrock *et al*, 2003; Dick *et al*, 2003; tom Dieck *et al*, 2005; Frank *et al*, 2010). Central glutamatergic synapses from these mice have no obvious structural defects, but do exhibit enhanced short-term depression and a high percentage of silent synapses (Hallermann *et al*, 2010). These milder phenotypes could result from a more ancillary role for Bassoon at central synapses, or from the significant structural and functional redundancy of the homologous Piccolo protein.

Recent studies of Piccolo-deficient neurons have uncovered similarly mild loss-of-function phenotypes (Leal-Ortiz *et al*, 2008; Mukherjee *et al*, 2010; Waites *et al*, 2011). For instance, RNAi knockdown of Piccolo has no effect on presynaptic ultrastructure, but enhances both activity-dependent SV exocytosis and synapsin1a dispersion out of presynaptic boutons (Leal-Ortiz *et al*, 2008), phenotypes now linked to Piccolo's role as a regulator of presynaptic F-actin assembly (Waites *et al*, 2011). In contrast, mice with a targeted deletion of exon 14 in the PCLO gene ($Pclo^{\Delta Ex14}$) exhibit no overt synaptic phenotypes, suggesting that Piccolo is dispensable for presynaptic function (Mukherjee *et al*, 2010). However, re-evaluation of these mice has revealed that they express multiple presynaptically localized Piccolo isoforms, indicating that exon 14 deletion causes only a partial loss of Piccolo protein (Waites *et al*, 2011). Consistent with this concept, shRNA-mediated knockdown of the remaining Piccolo isoforms from $Pclo^{\Delta Ex14}$ neurons robustly inhibits presynaptic F-actin assembly, suggesting that this phenotype only emerges upon near-complete elimination of Piccolo from boutons (Waites *et al*, 2011). Similarly, a subtle phenotype in SV clustering is reported in $Pclo^{\Delta Ex14}$ neurons

*Corresponding authors. CL Waites, Departments of Pathology and Cell Biology and Neuroscience, Columbia University Medical Center, Black Building 1210B, 630 West 168th Street, New York, NY 10032, USA. Tel.: +1 212 305 6025; Fax: +1 212 305 6595; E-mail: cw2622@columbia.edu or CC Garner, Nancy Pritzker Laboratory, Department of Psychiatry and Behavioral Sciences, Stanford University School of Medicine, Palo Alto, CA 94305, USA. Tel.: +1 650 723 4942; Fax: +1 650 498 7761; E-mail: cgarner@stanford.edu

Received: 26 July 2012; accepted: 15 January 2013; published online: 12 February 2013

expressing an shRNA that reduces Bassoon expression by ~70% (Mukherjee *et al*, 2010). However, it is likely that incomplete loss of both proteins yields a mild phenotype that underestimates their important shared functions within presynaptic boutons.

In the present study, we have re-examined these functions using well-characterized shRNAs that reduce expression of Bassoon and all Piccolo isoforms by >85%. Our analysis has uncovered a critical shared role for these molecules in regulating presynaptic ubiquitination and proteostasis. Specifically, Bassoon/Piccolo double knockdown (DKD) promotes the ubiquitination and degradation of presynaptic proteins, leading to synapse degeneration. This process is mediated in part by the E3 ubiquitin ligase Siah1, whose activity is negatively regulated via binding to the Bassoon and Piccolo zinc finger (ZF) domains. Together, our data demonstrate a novel function for Bassoon and Piccolo in maintaining synaptic integrity, and indicate that these proteins are important regulators of protein ubiquitination at the AZ.

Results

DKD of Bassoon and Piccolo with a tricistronic lentiviral vector

We previously characterized short-hairpin RNAs (shRNAs) that effectively knockdown Bassoon or Piccolo in cultured hippocampal neurons (Leal-Ortiz *et al*, 2008; Waites *et al*, 2011). To eliminate both proteins from neurons, we created a tricistronic lentiviral vector containing the Bassoon and Piccolo shRNAs driven by separate polymerase III promoters (U6 and H1, respectively), together with a reporter protein (ie. EGFP) driven by the Ubiquitin promoter (Figure 1A). We used a similar vector containing scrambled versions of both shRNAs as a control (EGFP/Scrambled Control or 'SC'). Since Bassoon and Piccolo are extremely stable proteins with long half-lives, we tested the double knockdown vector (EGFP/DKD) at three timepoints (9, 12, and 14–16 days *in vitro*; DIV) to determine when effective knockdown of both proteins was achieved. Lysates from dissociated hippocampal neurons transduced with high-titer lentivirus at the time of plating (for >80% infection) were harvested at these timepoints and subject to immunoblotting with antibodies against a series of synaptic proteins. These experiments revealed that EGFP/DKD significantly downregulated both Bassoon and Piccolo at 9 DIV (by ~75%), and further decreased their expression by 14–16 DIV (by ~90%; Figure 1B and C). Surprisingly, although the levels of all other pre- and postsynaptic proteins examined were similar in EGFP/SC and EGFP/DKD neurons at 9 DIV, they were significantly reduced in DKD neurons by 12 and 14–16 DIV (Figure 1B and C).

Loss of EGFP-SV2 fluorescence in presynaptic boutons lacking Bassoon and Piccolo

We first hypothesized that the loss of synaptic protein at 12–16 DIV resulted from poor neuronal health or abnormal development in the absence of Bassoon and Piccolo. However, DKD neurons did not exhibit decreased survival or abnormal dendritic morphology compared to SC neurons at 14–16 DIV (Supplementary Figure S1). We next theorized that this phenotype was due to an inability of axons lacking Bassoon and Piccolo to form synapses onto dendrites, leading to reduced synapse formation and the subsequent loss of synaptic proteins. We thus examined whether DKD axons could form presynaptic boutons.

To visualize boutons, we replaced soluble EGFP in the SC and DKD vectors with EGFP-SV2 (EGFP-SV2/SC or/DKD), an SV integral membrane protein whose localization is exclusively presynaptic (Bajjalieh *et al*, 1994; Leal-Ortiz *et al*, 2008). Neurons were transduced or electroporated with these vectors at the time of plating, and examined at 9 or 14 DIV. Surprisingly, we found that EGFP-SV2 still clustered in 9 and 14 DIV axons lacking Bassoon and Piccolo (Figure 2A and B), and that these clusters were synaptic based on their colocalization with the postsynaptic protein PSD-95 (Supplementary Figure S1). However, similar to our findings in Figure 1, we observed a dramatic loss of EGFP-SV2 fluorescence over time. At 9 DIV, EGFP-SV2 fluorescence intensity was similar in SC and DKD neurons (Figure 2A and E) despite the absence of Bassoon and Piccolo immunoreactivity from >70% of EGFP-SV2 puncta in DKD neurons (Figure 2A, C, and E). In contrast, by 14 DIV, EGFP-SV2 fluorescence intensity was dramatically less in DKD than in SC neurons (Figure 2B and F). Although the efficacy of Bassoon/Piccolo knockdown did increase between 9 and 14 DIV, as illustrated by the decreased colocalization of EGFP-SV2 puncta with Bassoon and Piccolo (from ~30 to <5%; Figure 2C and D), the reduction in EGFP-SV2 fluorescence intensity was even greater (>80%). Similar results were seen with other EGFP-tagged and endogenous pre- and postsynaptic proteins (Supplementary Figure S2), suggesting that knockdown of Bassoon and Piccolo led to a profound loss of synaptic material over time.

Expression of shRNA-resistant Bassoon rescues SV loss

To rule out off-target effects of these shRNAs, we examined whether the reduced levels of presynaptic EGFP-SV2 could be rescued by expressing full-length Bassoon in the DKD background. Neurons were electroporated with EGFP-SV2/SC or/DKD vectors prior to plating, then transduced with shRNA-resistant, RFP-tagged Bassoon (RFP-Bsn*) at 5 DIV. The ability of RFP-Bsn* to rescue DKD-induced SV loss was assessed at 14 DIV. RFP-Bsn* was introduced into neurons via helper-dependent, non-replicating adenovirus (Palmer and Ng, 2011), which enabled the efficient (>40%) infection of hippocampal neurons with this ~14 kb cDNA. Reassuringly, we found that RFP-Bsn* expression prevented the dramatic loss of EGFP-SV2 fluorescence seen in DKD boutons (Figure 3A–C). Synaptophysin immunoreactivity was also maintained at levels similar to those observed in SC boutons, indicating that the effect was not specific for EGFP-SV2 (Figure 3D and E). These findings indicated that off-target effects of the shRNAs were not responsible for the loss of presynaptic proteins over time, as recombinant Bassoon expression alone rescued this phenotype.

Degeneration of Bassoon/Piccolo-deficient boutons

To examine the ultrastructure of Bassoon/Piccolo-deficient boutons, we used SC and DKD vectors containing the SV integral membrane protein VAMP2 conjugated to horseradish peroxidase (VAMP2-HRP). As previously demonstrated (Leal-Ortiz *et al*, 2008; Hua *et al*, 2011), VAMP2-HRP forms an electron-dense precipitate within SVs, thereby facilitating the

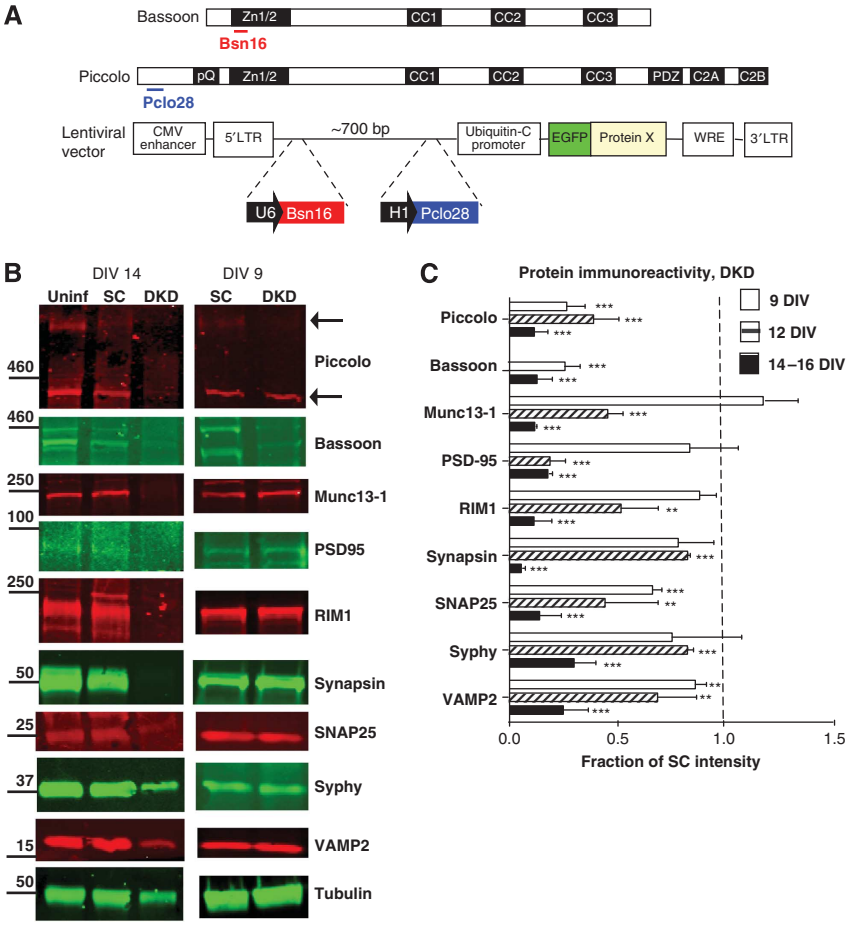

Figure 1 Loss of synaptic proteins from Bassoon/Piccolo DKD neurons. (**A**) Schematic diagram showing regions targeted by Bassoon and Piccolo shRNAs (Bsn16 and Pclo28) and the tricistronic lentiviral vector used to express them. EGFP/EGFP-tagged reporter proteins are driven by the Ubiquitin C promoter, while Bsn16 and Pclo28 are driven by polymerase III promoters (U6 and H1, respectively) and separated by 700 bp of stuffer sequence. (**B**) Immunoblots of lysates from 9 or 14 day *in vitro* (DIV) neurons transduced with nothing (uninf), scrambled control shRNAs for Bassoon and Piccolo (SC), or Bsn 16 and Pclo28 shRNAs (DKD) at the time of plating. Samples were probed with the antibodies indicated (syphy = synaptophysin). Protein size markers are in kDa. Arrows indicate two most prominent Piccolo isoforms. (**C**) Quantification of synaptic protein immunoreactivity in 9, 12, and 14–16 DIV lysates. Values were measured by densitometry, normalized to tubulin, and expressed as fraction of SC intensity (indicated by dashed line; $***P<0.0001$, $**P<0.005$, unpaired *t*-test; $n \geqslant 3$ experiments/timepoint).Source data for this figure is available on the online supplementary information page.

identification of SC and DKD boutons by electron microscopy (EM). Similarly to previous experiments, neurons were electroporated with VAMP2-HRP/SC and/DKD constructs prior to plating and processed for EM analysis on 9 or 14 DIV. As anticipated, presynaptic boutons expressing the SC vector were morphologically normal at both timepoints, containing many ~40 nm diameter SVs of uniform density juxtaposed to prominent postsynaptic densities (PSDs) (Figure 4A, C, and E). In contrast, DKD boutons had many abnormal features that became more pronounced over time. For example, while 9 DIV DKD boutons often had multiple 40 nm SVs juxtaposed to an identifiable PSD (Figure 4B), they also contained significantly more pleiomorphic vesicles and abnormally elongated/enlarged SVs compared to their SC counterparts (Figure 4B–D). Moreover, juxtaposed PSDs were noticeably less electron dense (Figure 4B and E). At 14 DIV, DKD boutons were even less recognizable. Although varicosities containing a few 40 nm SVs could be identified, most contained a variety of pleiomorphic vesicles >80 nm in diameter (Figure 4D). Some of these were tubulovesicular structures resembling early endosomes (Parton *et al*, 1992), while others were spherical and reminiscent of late endosomes/multi-vesicular bodies (MVBs) known to transport organelles and proteins to lysosomes for degradation (Almeida *et al*, 2006; Altick *et al*, 2009; Lee *et al*, 2011; Figure 4B). Surprisingly, juxtaposed PSDs were almost uniformly absent at 14 DIV, suggesting that the integrity of postsynaptic structures was ultimately affected by presynaptic loss of Bassoon and Piccolo (Figure 4E). Together, these data indicated that Bassoon/Piccolo knockdown led to a profound disintegration of synapses, and that this process began at a relatively early timepoint (9 DIV in our cultures).

Upregulation of endo-lysosomal organelles in DKD neurons

The large number of tubulovesicular and MVB-like structures observed in DKD neurons suggested that endo-lysosomal organelles were upregulated in these cells. To test this concept, we performed two experiments. First, 14 DIV neurons transduced with EGFP/SC or/DKD constructs at the time of plating were incubated with LysoTracker Red to label lyso-

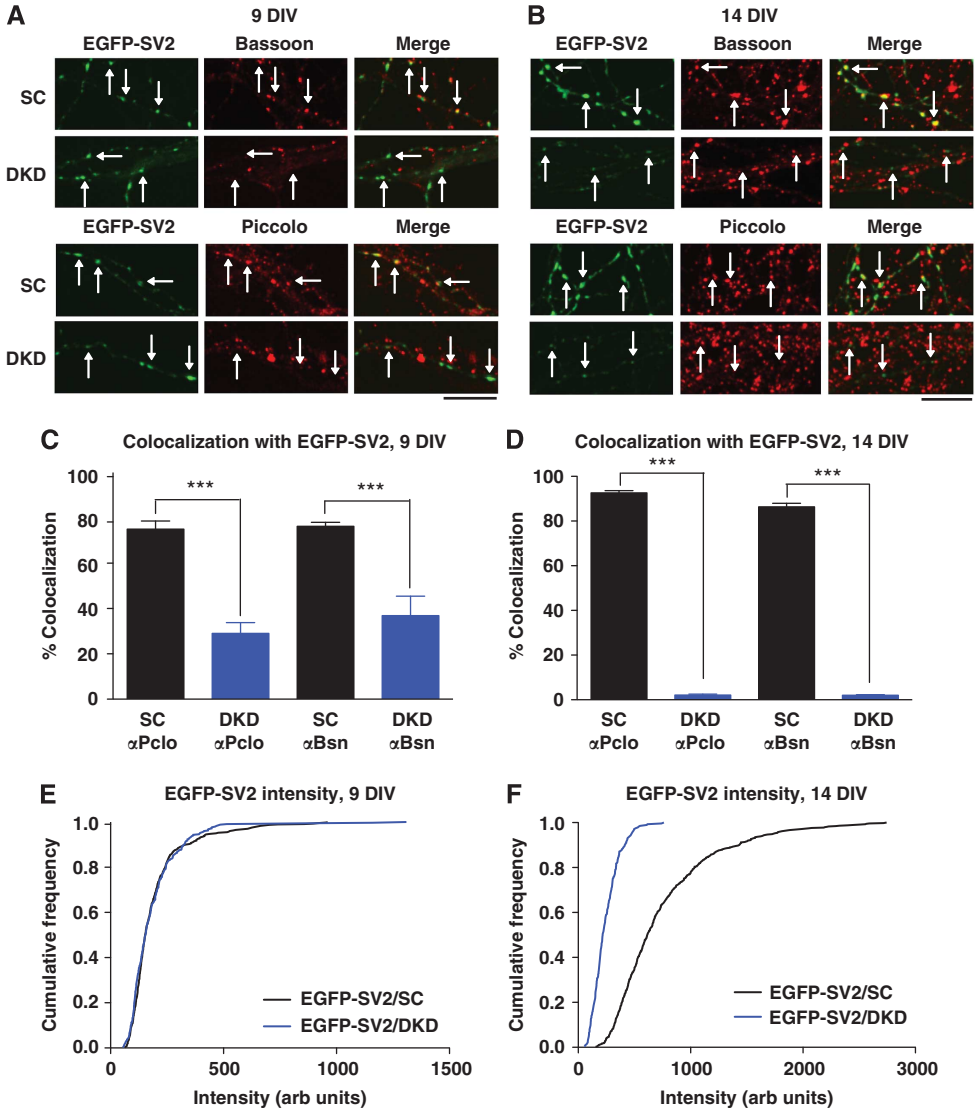

Figure 2 Loss of SVs from Bassoon/Piccolo DKD boutons. (**A**) Nine DIV neurons transduced with EGFP-SV2/SC or/DKD at the time of plating (to infect ~20% of neurons) and immunostained with Bassoon or Piccolo antibodies. Bassoon and Piccolo immunoreactivity are present within the boutons of SC but not of DKD neurons (white arrows). Size bar is 10 μm. (**B**) Same as (**A**), but with 14 DIV neurons. EGFP-SV2 fluorescence is dramatically reduced in the DKD condition. Size bar is 10 μm. (**C**) EGFP-SV2 colocalization with Bassoon and Piccolo at 9 DIV for SC and DKD conditions. Only ~30% of EGFP-SV2 puncta have Bassoon or Piccolo immunoreactivity in DKD neurons, versus 80% for SC ($n \geqslant 4$ fields of view/condition, with >50 puncta/field; $^{***}P < 0.0001$, unpaired *t*-test. (**D**) Same as (**C**), but for 14 DIV neurons. More than 5% of EGFP-SV2 puncta colocalize with Bassoon and Piccolo in DKD boutons, versus ~90% in SC boutons ($n \geqslant 4$ fields of view/condition, >50 puncta/field; $^{***}P < 0.0001$, unpaired *t*-test. (**E**) Cumulative frequency distribution of EGFP-SV2 fluorescence intensity in SC and DKD boutons on 9 DIV. The distribution is similar for both conditions ($n = 400$ SC and 350 DKD boutons, $\geqslant 8$ fields of view/condition). (**F**) Same as (**E**), but for 14 DIV neurons. The distribution of EGFP-SV2 fluorescence is now significantly shifted to the left for DKD boutons, indicating smaller SV pool size per synapse ($n = 590$ SC and 280 DKD boutons, $\geqslant 8$ fields of view/condition).

somes, and subject to live imaging. Interestingly, we found that DKD neurons had significantly more LysoTracker puncta/cell body than SC neurons (Figure 5A and B). Moreover, these puncta were often concentrated in the initial segment of the axon, potentially facilitating the degradation of retrogradely transported presynaptic proteins and membranes (Figure 5A). In a second experiment, 14 DIV EGFP/SC and/DKD neurons were immunostained with antibodies against CHMP2b, a component of the ESCRT complex involved in the formation and retrograde transport of MVBs. As with lysosomes, significantly more CHMP2b immunoreactivity was found in DKD cell bodies and axons (Figure 5C and D), consistent with an increased number of endo-lysosomal structures in these neurons.

Increased protein ubiquitination and degradation in DKD neurons

Our findings indicated that protein degradation was enhanced in Bassoon/Piccolo-deficient neurons. We therefore assessed whether DKD-induced protein loss could be blocked by inhibitors of lysosomes or proteasomes, the two major cellular organelles responsible for protein degradation (Waites and Garner, 2011). At 12 DIV, EGFP-SV2/SC and/DKD-expressing neurons were incubated for 16 h with

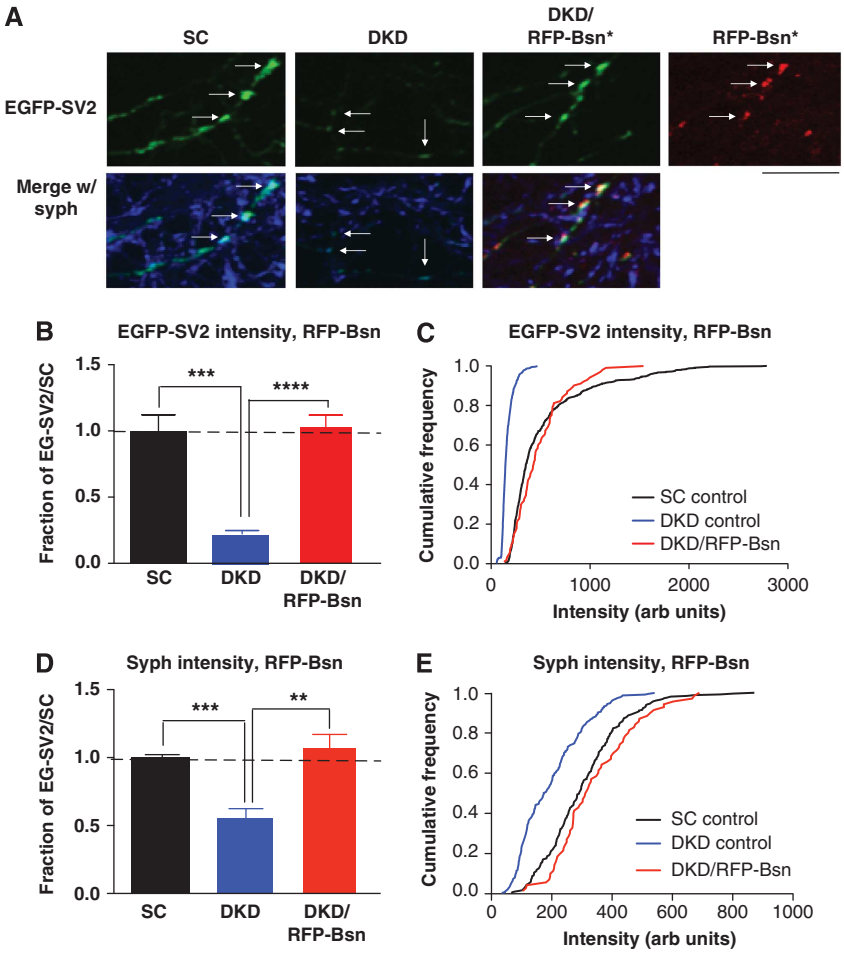

Figure 3 Rescue of DKD phenotype by shRNA-resistant Bassoon. (**A**) Fourteen DIV neurons expressing EGFP-SV2/SC, EGFP-SV2/DKD, or EGFP-SV2/DKD and shRNA-resistant RFP-Bassoon (RFP-Bsn*), immunostained with synaptophysin antibodies. RFP-Bsn* rescues the loss of EGFP-SV2 and synaptophysin from DKD boutons. Size bar is 10 μm. (**B**) EGFP-SV2 intensity at boutons expressing SC, DKD, or DKD/RFP-Bsn*. Values are expressed as fraction of EGFP-SV2 intensity at SC boutons (dashed line). EGFP-SV2 intensity is reduced by ~80% in the DKD background, but rescued to control levels in the presence of RFP-Bsn* ($n \geqslant 4$ fields of view/condition, >100 boutons/field; $^{***}P<0.0005$, $^{****}P<0.0001$, unpaired *t*-test). (**C**) Cumulative frequency distribution of EGFP-SV2 fluorescence intensity at SC, DKD, or DKD + RFP-Bsn* boutons. This curve is left-shifted in DKD neurons, but similar to SC in the presence of RFP-Bsn*. Values are from (**B**) ($n = 673$ SC, 541 DKD, and 101 DKD/RFP-Bsn* boutons, ⩾4 fields of view/condition). (**D**) Like (**B**) but for synaptophysin, which is reduced by ~50% in the DKD background and rescued to control levels by RFP-Bsn* ($n \geqslant 3$ fields of view/condition, >50 boutons/field; $^{**}P<0.005$, $^{***}P<0.0001$, unpaired *t*-test). (**E**) Similar to (**C**), for synaptophysin. Again, the curve is left-shifted in the DKD condition, but similar to SC in the presence of RFP-Bsn*. Values are from (**D**) ($n = 261$ SC, 236 DKD, and 70 DKD/RFP-Bsn* boutons, ⩾3 fields of view/condition).

200 μM chloroquine/100 μM leupeptin (chloro/leu) or 0.1 μM epoxomicin to inhibit lysosomal or proteasomal activity, respectively (Ehlers, 2003; Lee *et al*, 2004; Willeumier *et al*, 2006). EGFP-SV2 fluorescence intensity was then compared in treated versus untreated neurons. Interestingly, we found that chloro/leu treatment completely prevented the loss of EGFP-SV2 fluorescence in DKD boutons, but had no effect on its fluorescence in SC boutons over this time period (Figure 6A, B, and E). Epoxomicin treatment similarly increased EGFP-SV2 fluorescence in the DKD but not in the SC background (Figure 6A, C, and F). To confirm that degradation was responsible for DKD-induced presynaptic protein loss, we monitored the loss of VAMP2, SNAP-25, and Munc13 from EGFP/SC and/DKD-expressing neurons treated with the protein synthesis inhibitor cycloheximide for 0, 12, and 24 h. Lysates from DKD neurons exhibited significantly less immunoreactivity for all three proteins following 24 h of cycloheximide treatment (Supplementary Figure S3), demonstrating that rates of presynaptic protein degradation were increased upon Bassoon/Piccolo knockdown.

Most proteins are targeted for degradation via ubiquitination, a post-translational modification wherein one or more ubiquitin molecules are covalently attached to a specific lysine residue of the target protein (Varshavsky, 2005; Yi and Ehlers, 2005; Waites and Garner, 2011). Attachment of four or more ubiquitin molecules (polyubiquitination) typically leads to degradation via the proteasome, while monoubiquitination can target proteins to the endo-lysosomal pathway. Ubiquitination requires the coordinated activity of E1 ubiquitin activating enzymes, E2 ubiquitin conjugating enzymes, and E3 ubiquitin ligases (Ding and Shen, 2008; Lehman, 2009). To test whether DKD-mediated protein degradation required ubiquitination, neurons expressing the EGFP-SV2/SC and/DKD constructs were treated for 16 h (from 12 to 13 DIV) with 1 μM ziram, a drug that blocks the E1 ubiquitin activating enzyme

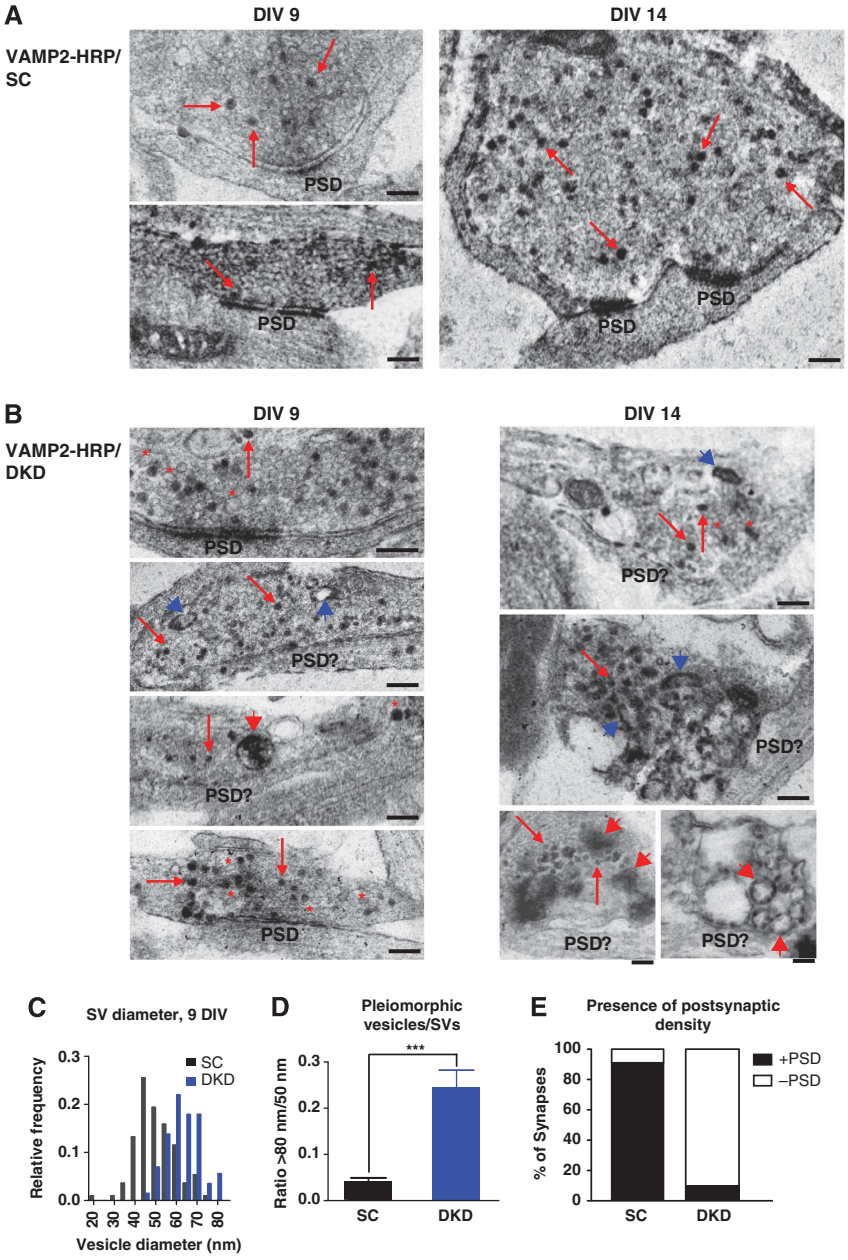

Figure 4 Pronounced degeneration of DKD-expressing boutons. (**A**) Electron micrographs of boutons expressing VAMP2-HRP/SC at 9 (left) or 14 (right) DIV. Red arrows indicate SVs labelled with electron-dense VAMP2-HRP. PSD, postsynaptic density. (**B**) Boutons expressing VAMP2-HRP/DKD at 9 (left) or 14 (right) DIV. Red arrows indicate labelled SVs, red asterisks (above vesicles) indicate irregular-shaped SVs, blue arrowheads indicate tubulovesicular structures, and red arrowheads indicate structures resembling multi-vesicular bodies (MVBs). Note the increase in tubulovesicular and MVB-like structures, and concomitant decrease in SVs, at 14 versus 9 DIV. Also note the lack of PSDs at 14 DIV DKD boutons. Size bars are 200 nm. (**C**) Relative frequency histogram of SV diameters in SC versus DKD boutons at 9 DIV. DKD boutons have larger SV diameters ($n = 114$ SVs from 5 boutons for SC and 146 SVs from 10 boutons for DKD). (**D**) Ratio of pleiomorphic vesicles (>80 nm diameter) to SVs (30–70 nm diameter) per bouton for SC and DKD-expressing boutons. Clearly identifiable, VAMP2-HRP-labelled boutons from 9 and 14 DIV neurons were included in this analysis. DKD boutons have a significantly larger average ratio, reflecting their increased number of pleiomorphic vesicles and decreased number of SVs ($n = 33$ SC and 45 DKD boutons from two independent experiments; $^{***}P < 0.0005$, unpaired *t*-test). (**E**) Percentage of SC and DKD synapses containing an identifiable PSD. Clearly recognizable postsynaptic compartments juxtaposed to VAMP2-HRP labelled, vesicle-containing varicosities (from 9 and 14 DIV neurons) were included in this analysis ($n = 33$ SC and 40 DKD synapses from two independent experiments).

(Chou *et al*, 2008; Rinetti and Schweizer, 2010). As with chloro/leu and epoxomicin, ziram significantly increased EGFP-SV2 fluorescence at DKD but not at SC boutons (Figure 6A, D, and G), suggesting that protein ubiquitination was enhanced at Bassoon/Piccolo-deficient boutons.

To determine whether DKD-induced protein degradation was mediated primarily by mono- or polyubiquitination, we overexpressed 'knockout' (KO) ubiquitin, in which all lysines were replaced with arginines to prevent polyubiquitin linkage formation (Lim *et al*, 2005). Neurons were co-transduced at the time of plating with EGFP-SV2/SC or/DKD together with a construct that stoichiometrically co-expresses KO ubiquitin and soluble mCherry. EGFP-SV2 fluorescence intensity was then assessed at 14 DIV in the presence or absence

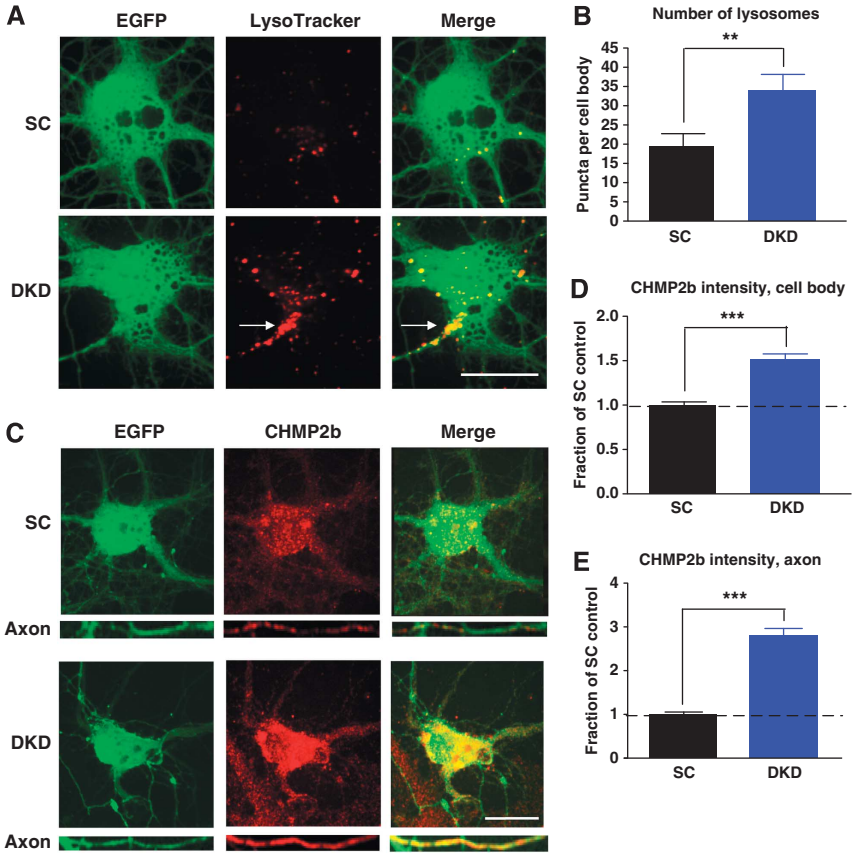

Figure 5 Increased number of endo-lysosomal organelles in DKD neurons. (**A**) Fourteen DIV neurons transduced with EGFP/SC or/DKD at the time of plating and incubated with LysoTracker Red to label lysosomes. Note the increased accumulation of lysosomes in DKD neurons, particularly in the initial segment of the axon (white arrows). Size bar is 20 μm. (**B**) Lysosome number per cell body. DKD neurons have nearly twice as many lysosomes as SC neurons ($n = 22$ cells for SC, 18 cells for DKD, 3 experiments; $^{**}P < 0.005$). (**C**) Fourteen DIV neurons fixed and immunostained with antibodies to CHMP2b, a component of multi-vesicular bodies. CHMP2b is significantly elevated in cell bodies and axons of DKD versus SC neurons. Size bar is 20 μm. (**D**, **E**) CHMP2b immunofluorescence intensity, expressed as fraction of fluorescence intensity in SC cell bodies (**D**) and axons (**E**) (dashed line). DKD neurons exhibit ~50 and 150% more CHMP2b fluorescence in their somas and axons, respectively, than SC neurons ($n = 10$–20 cells/condition, experiment repeated four times; $^{***}P < 0.0001$).

of mCherry/KO ubiquitin. Interestingly, KO ubiquitin overexpression led to significantly increased (~25%) EGFP-SV2 fluorescence in control (SC) neurons (Figure 7A–C), indicating that polyubiquitination typically mediates SV2 degradation. Similarly, KO ubiquitin increased EGFP-SV2 fluorescence in DKD boutons by almost 40% (Figure 7A–C). Synaptophysin and VAMP2 immunofluorescence were increased by nearly identical amounts (Supplementary Figure S4), demonstrating that polyubiquitination mediates DKD-induced protein degradation for at least a subset of presynaptic proteins.

To confirm that protein polyubiquitination was increased in Bassoon/Piccolo-deficient boutons, we performed several immunoprecipitation experiments. We first immunoprecipitated VAMP2 and synaptophysin from synaptosomes isolated from 9 DIV SC or DKD-expressing neurons (treated with proteasome and lysosome inhibitors for 8 h), and assessed their ubiquitination states. For both proteins, immunoprecipitated material from DKD neurons had more ubiquitin immunoreactivity on the portion of the blot corresponding to >100 kDa molecular weight (Figure 7D and E). To determine whether these bands could represent polyubiquitinated synaptophysin and VAMP2, we subsequently immunoprecipitated these proteins from wild-type neurons (± proteasome and lysosome inhibitors), and immunoblotted this material with a different set of synaptophysin or VAMP2 antibodies. Similar high molecular weight bands appeared on these blots *only* in the presence of proteasome/lysosome inhibitors (Figure 7D and E, arrows), indicating that they likely represented polyubiquitinated forms of synaptophysin and VAMP2. Together, these data demonstrate that Bassoon/Piccolo DKD promotes protein polyubiquitination within the presynaptic compartment.

Bassoon and Piccolo interact with the E3 ubiquitin ligase Siah1

How does the loss of two AZ-associated proteins lead to enhanced presynaptic protein ubiquitination? One possibility is that Bassoon and Piccolo regulate presynaptic ubiquitinating enzymes. Of these, the most plausible candidates are E3 ligases, which provide substrate specificity and exhibit restricted spatial and temporal expression patterns. Intriguingly, the E3 ligase Siah1 had previously been identified in a yeast two-hybrid screen for Bassoon interacting partners (Supplementary Figure S5). Siah1 was particularly interesting to us in the context of presynaptic protein degradation because it is expressed in neurons (Moriyoshi *et al*, 2004) and a number of its targets (synaptophysin, β-catenin,

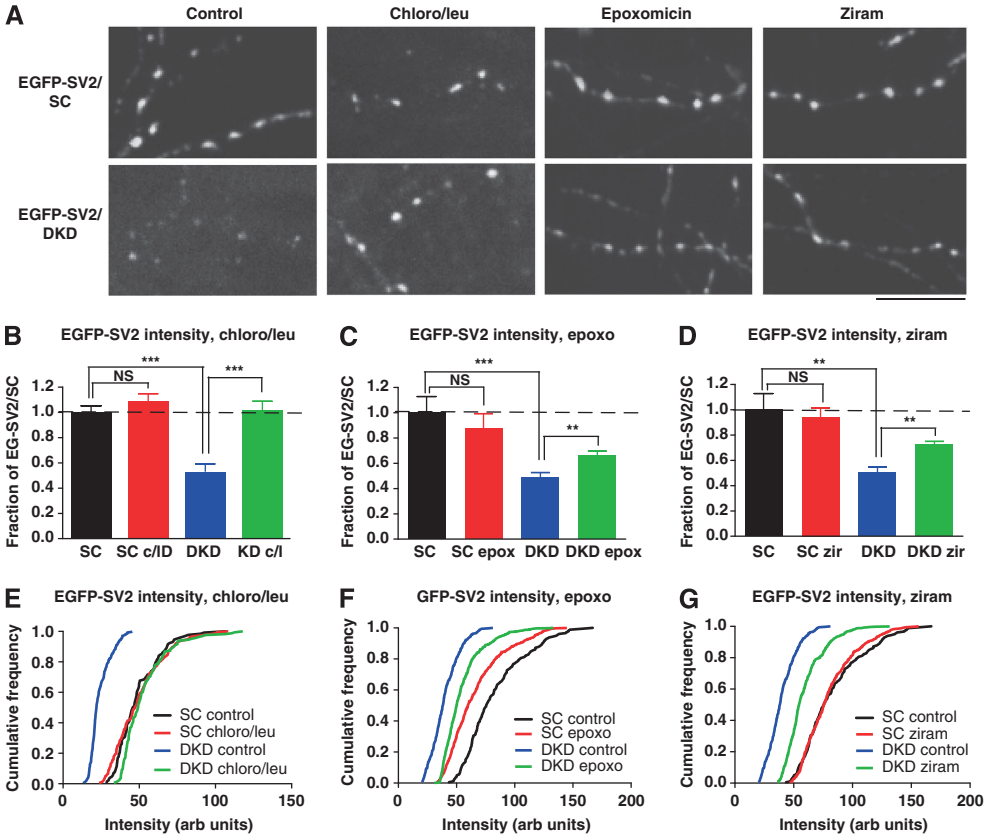

Figure 6 Protein degradation drives DKD-induced bouton loss. (**A**) Thirteen DIV neurons transduced with EGFP-SV2/SC or/DKD at the time of plating, untreated (control) or treated for 16 h with 200 μM chloroquine/100 μM leupeptin to block lysosomal degradation, 0.1 μM epoxomicin to block the proteasome, or 1 μM ziram to block protein ubiquitination. All treatments increase EGFP-SV2 fluorescence in the DKD but not in the SC background. Size bar is 10 μm. (**B**) EGFP-SV2 fluorescence intensity in SC or DKD boutons treated with chloro/leu. Values are expressed as fraction of EGFP-SV2 intensity at untreated SC boutons (dashed line). Chloro/leu treatment prevents the ~50% loss of EGFP-SV2 fluorescence at DKD boutons, but has no effect on SC boutons ($n=3$ fields of view/condition, >50 boutons/field; $^{***}P<0.001$, unpaired *t*-test). Results confirmed in three independent experiments. (**C**) Similar to (**B**), but for epoxomicin, which boosts EGFP-SV2 fluorescence by ~20% in the DKD background, but has no significant effect on SC boutons ($n>3$ fields of view/condition, >60 boutons/field; $^{***}P<0.001$, $^{**}P<0.005$, unpaired *t*-test). Results confirmed in three independent experiments. (**D**) Similar to (**B**), but for ziram, which boosts EGFP-SV2 fluorescence in the DKD background by ~20% but does not affect EGFP-SV2 intensity in SC boutons ($n>3$ fields of view/condition, >60 boutons/field; $^{**}P<0.009$, unpaired *t*-test). Results confirmed in three experiments. (**E**) Cumulative frequency distribution of EGFP-SV2 intensity at SC and DKD boutons treated with chloro/leu. The DKD curve is significantly left-shifted, but chloro/leu treatment shifts the DKD intensity distribution to match those of the SC conditions. Values are from (**B**) ($n=130$ SC control, 181 SC chloro/leu, 269 DKD control, and 166 DKD chloro/leu boutons). (**F**) Similar to (**E**), but for epoxomicin, which also shifts the DKD curve to the right, indicating some rescue of the phenotype. Values are from (**C**) ($n=180$ SC control, 350 DKD control, 469 SC epoxomicin, and 611 DKD epoxomicin boutons). (**G**) Similar to (**E**) and (**F**), but for ziram, which also shifts the DKD curve to the right. Values are from (**D**) ($n=180$ SC control, 350 DKD control, 551 SC/ziram, and 495 DKD/ziram boutons).

α-synuclein, synphilin-1) are SV-associated proteins (Liu *et al*, 2001; Wheeler *et al*, 2002; Liani *et al*, 2004; Santelli *et al*, 2005; Szargel *et al*, 2009; Dimitrova *et al*, 2010). In addition, the region of Bassoon shown to interact with Siah1 by yeast two-hybrid, the N-terminal domain containing amino acids 1–609 (Supplementary Figure S5), has two ZFs that are also present in Piccolo (Figure 8A). We therefore performed a series of experiments to confirm the interactions between Bassoon/Piccolo and Siah1.

We first performed co-immunoprecipitation assays in HEK cells co-transfected with myc-Siah1 and each of the four ZFs tagged with mCherry. All four ZFs were pulled down with myc-Siah1 (Figure 8B), demonstrating that Siah1 interacts with both Bassoon and Piccolo ZFs. Full-length RFP-Bassoon was also co-immunoprecipitated with myc-Siah1, as evidenced by the multiple proteolytic fragments between 460 and 50 kD, all of which reacted with both mCherry and Bassoon antibodies (Figure 8C). In contrast, RFP-synapsin1a, another presynaptic protein, was never pulled down by myc-Siah1 (Figure 8C).

Siah1 contains a structurally conserved RING domain that interacts with E2 ubiquitin conjugating enzymes to facilitate protein ubiquitination (Santelli *et al*, 2005). One way that Bassoon and Piccolo could regulate Siah1 function is by interacting with its RING domain, thereby competing with E2 enzymes and inhibiting Siah1's ubiquitinating activity. To test this possibility, EGFP-tagged RING or Sina domains of Siah1 (Figure 8A) were used to co-immunoprecipitate mCh-ZF1 of Bassoon (Bsn) following their co-transfection into HEK cells. Bsn ZF1 was more robustly co-immunoprecipitated with the RING than the Sina domain (Figure 8D), although neither bound as effectively as full-length Siah1 (Figure 8B), implying that sequences outside of the RING domain also contribute to efficient Siah1/ZF binding. Nonetheless, this experiment suggested that the ZFs may inhibit Siah1-mediated ubiquitination by interfering with the E2

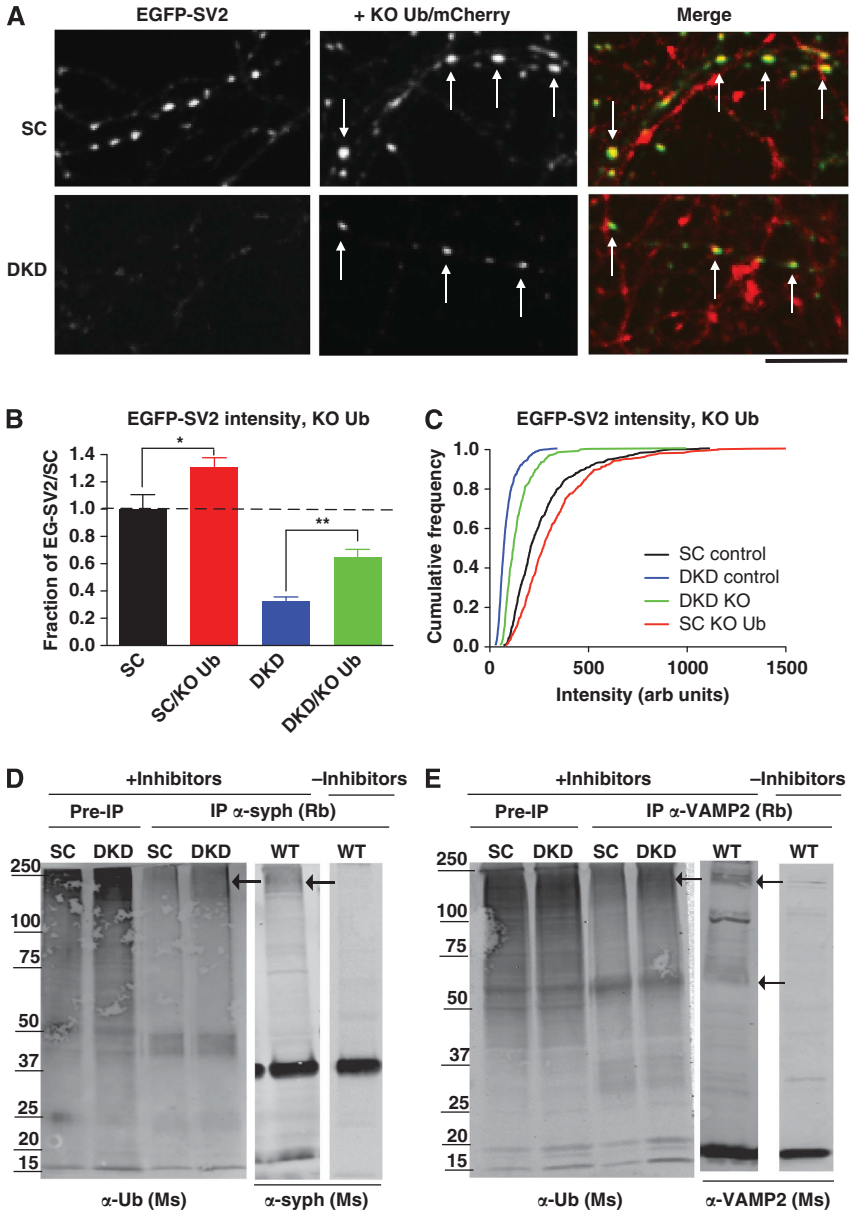

Figure 7 Increased protein polyubiquitination in DKD boutons. (**A**) Fourteen DIV neurons singly transduced with EGFP-SV2/SC or/DKD at the time of plating, or co-transduced with EGFP-SV2/SC or/DKD and knockout ubiquitin expressed together with mCherry (+KO Ub/mCherry). Arrows indicate EGFP-SV2 puncta that colocalize with KO Ub in presynaptic boutons. EGFP-SV2 fluorescence in the DKD background is increased by KO Ub, which inhibits polyubiquitination. (**B**) EGFP-SV2 intensity in SC and DKD boutons ±KO Ub. Values are expressed as fraction of EGFP-SV2 intensity at untreated SC boutons (dashed line). KO Ub increases EGFP-SV2 fluorescence by ⩾30% at both SC and DKD boutons ($n \geqslant 4$ fields of view/condition, >50 puncta/field; $^{*}P<0.05$, $^{**}P<0.005$, unpaired *t*-test). Results confirmed in three independent experiments. (**C**) Cumulative frequency distribution of EGFP-SV2 intensity at SC and DKD boutons ±KO Ub. Both SC and DKD curves are shifted to the right by KO Ub, indicating that EGFP-SV2 degradation is inhibited ($n=608$ SC control, 655 DKD control, 438 SC+KO Ub, 420 DKD+KO Ub). (**D**) Immunoblots of synaptosomes prepared from wild-type (WT), SC, or DKD-expressing neurons ±8 h treatment with epoxomicin and chloro/leu (±inhibitors). Total or synaptophysin-immunoprecipitated (IP α-syph) material was probed with monoclonal antibodies against ubiquitin (Ub) or synaptophysin. Equal protein concentrations were loaded for SC and DKD conditions. More ubiquitin immunoreactivity is associated with synaptophysin immunoprecipitates from DKD neurons (arrow). This material likely represents polyubiquitinated synaptophysin, as a similar-sized smear is recognized by synaptophysin antibodies in WT neurons (arrow), and is only present following proteasome/lysosome inhibition. The asterisk denotes non-ubiquitinated protein. (**E**) Similarly to (**D**), but for VAMP2. More ubiquitin immunoreactivity is also associated with VAMP2 immunoprecipitated from DKD neurons. Source data for this figure is available on the online supplementary information page.

enzyme-RING domain interaction. The ability of Bsn ZF1 to inhibit Siah1-mediated ubiquitination was examined by co-expressing HA-Ubiquitin and a Siah1 substrate (synaptophysin) in HEK cells, and assessing ubiquitination in the presence or absence of myc-Siah1 and mCh-Bsn ZF1 (Supplementary Figure S5). Bsn ZF1 significantly attenuated Siah1-mediated ubiquitination of synaptophysin (Supplementary Figure S5), consistent with a model wherein the Bassoon/Piccolo ZF domains negatively regulate Siah1 function by interfering with its ubiquitinating activity.

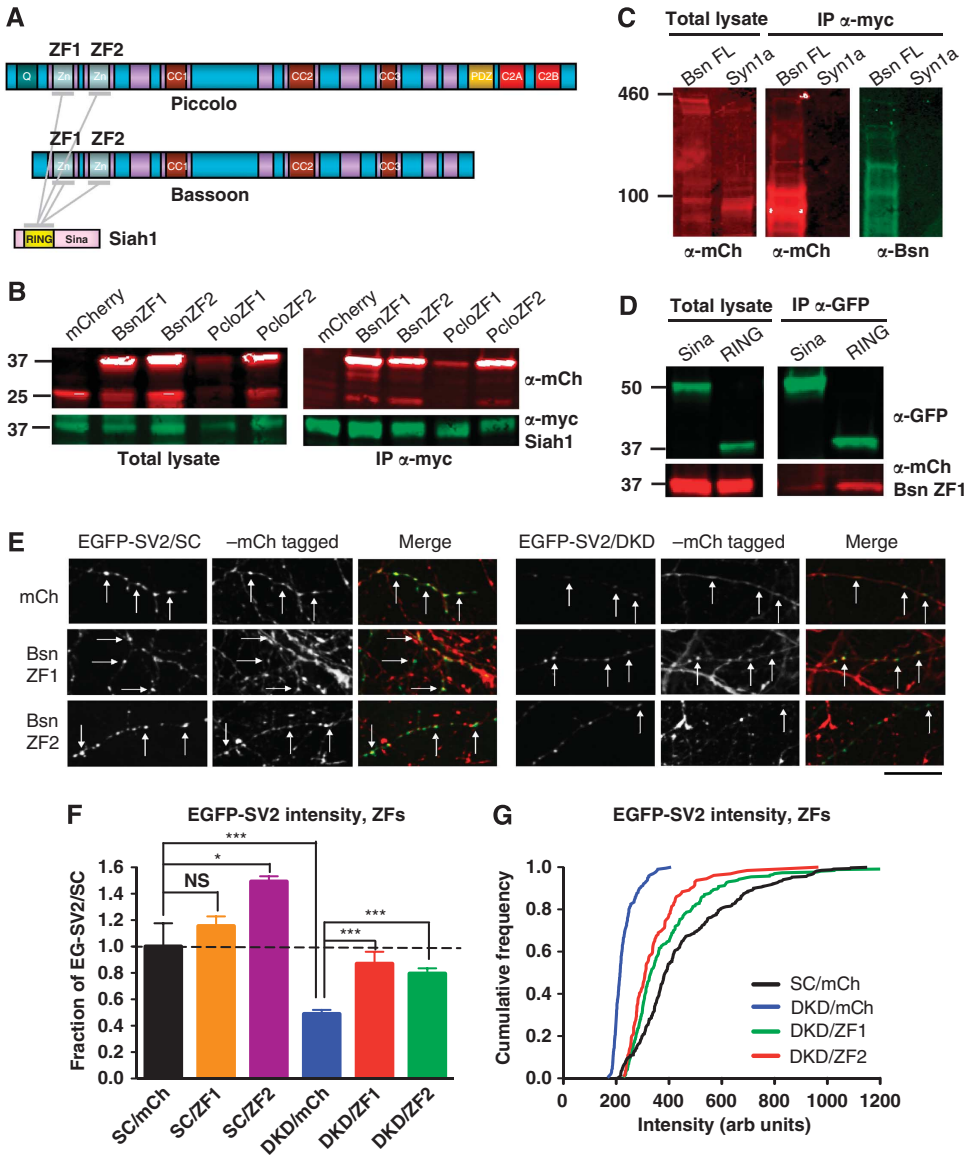

Figure 8 Bassoon and Piccolo zinc finger domains interact with Siah1 and ameliorate bouton loss. (**A**) Schematic diagram showing the interacting domains of Piccolo, Bassoon, and Siah1. Piccolo and Bassoon each have two zinc finger domains (ZF1 and ZF2), and all four of these interact with Siah1's RING domain. (**B**) Co-immunoprecipitation (co-IP) of mCherry (mCh)-Bassoon and Piccolo ZFs with myc-Siah1. Left panels show immunoreactivity from total HEK cell lysates, and right panels from anti-myc immunoprecipitates. Protein size markers are indicated. Similar results were obtained in three independent experiments. (**C**) Co-IP of mCh-tagged full-length Bassoon (Bsn FL), but not mCh-Synapsin1a, with myc-Siah1. Total lysates (left) were probed with mCh antibody, and anti-myc immunoprecipitates (middle and right) with mCh or Bassoon antibody. Protein size markers are indicated. (**D**) Co-IPs of mCh-tagged Bassoon ZF1 (BsnZF1) with EGFP-tagged Sina or RING domains of Siah1. BsnZF1 is more effectively co-immunoprecipitated with the RING domain, suggesting a stronger interaction with this region of Siah1. (**E**) Images of 14 DIV neurons expressing EGFP-SV2/SC or/DKD together with either soluble mCherry or mCh-tagged ZF1 or ZF2 of Bassoon. Arrows indicate colocalization of these proteins within presynaptic boutons. Size bar is 10 μm. (**F**) EGFP-SV2 fluorescence intensity in SC or DKD boutons co-expressing soluble mCh, mCh-BsnZF1, or mCh-BsnZF2. Both ZFs partially rescue EGFP-SV2 fluorescence loss in the DKD background (by >30%) and ZF2 significantly increases EGFP-SV2 fluorescence in SC boutons ($n \geqslant 3$ fields of view/condition, >60 boutons/field; $^{***}P<0.0005$, $^{*}P<0.05$, unpaired *t*-test). Results were confirmed in three independent experiments. (**G**) Cumulative frequency distribution of EGFP-SV2 fluorescence intensity in DKD boutons expressing mCh-ZF1 or 2. Both partially rescue the loss of EGFP-SV2 fluorescence, shifting the intensity distribution towards the right. The distribution of EGFP-SV2 in SC boutons expressing soluble mCherry is shown for comparison (black curve). Values are from (**F**) ($n = 350$ SC/mCh, 215 DKD/mCh, 260 DKD/mCh-BsnZF1, 130 DKD/mCh-BsnZF2 boutons). Source data for this figure is available on the online supplementary information page.

A prediction of this model is that overexpression of the Bassoon or Piccolo ZFs should suppress DKD-induced SV loss. To test this prediction, neurons were co-transduced with EGFP-SV2/SC or/DKD and either mCherry or mCherry-tagged Bsn ZF1 or ZF2. The ZF constructs exhibited relatively diffuse expression patterns in cell bodies and dendrites, but accumulated in axonal varicosities and exhibited a high degree of colocalization with EGFP-SV2 (Figure 8E). Intriguingly, while mCherry alone had no effect on presynaptic EGFP-SV2 fluorescence intensity/bouton in either background, each of the Bsn ZFs partially rescued the loss of EGFP-SV2 fluorescence at DKD boutons (by ~35%;

Figure 8E–G). Moreover, Bsn-ZF2 significantly increased EGFP-SV2 fluorescence intensity in SC boutons (Figure 8F), suggesting that these domains are important regulators of SV pool size. Both Piccolo ZFs exhibited similar effects, suggesting a common function for these domains (Supplementary Figure S5).

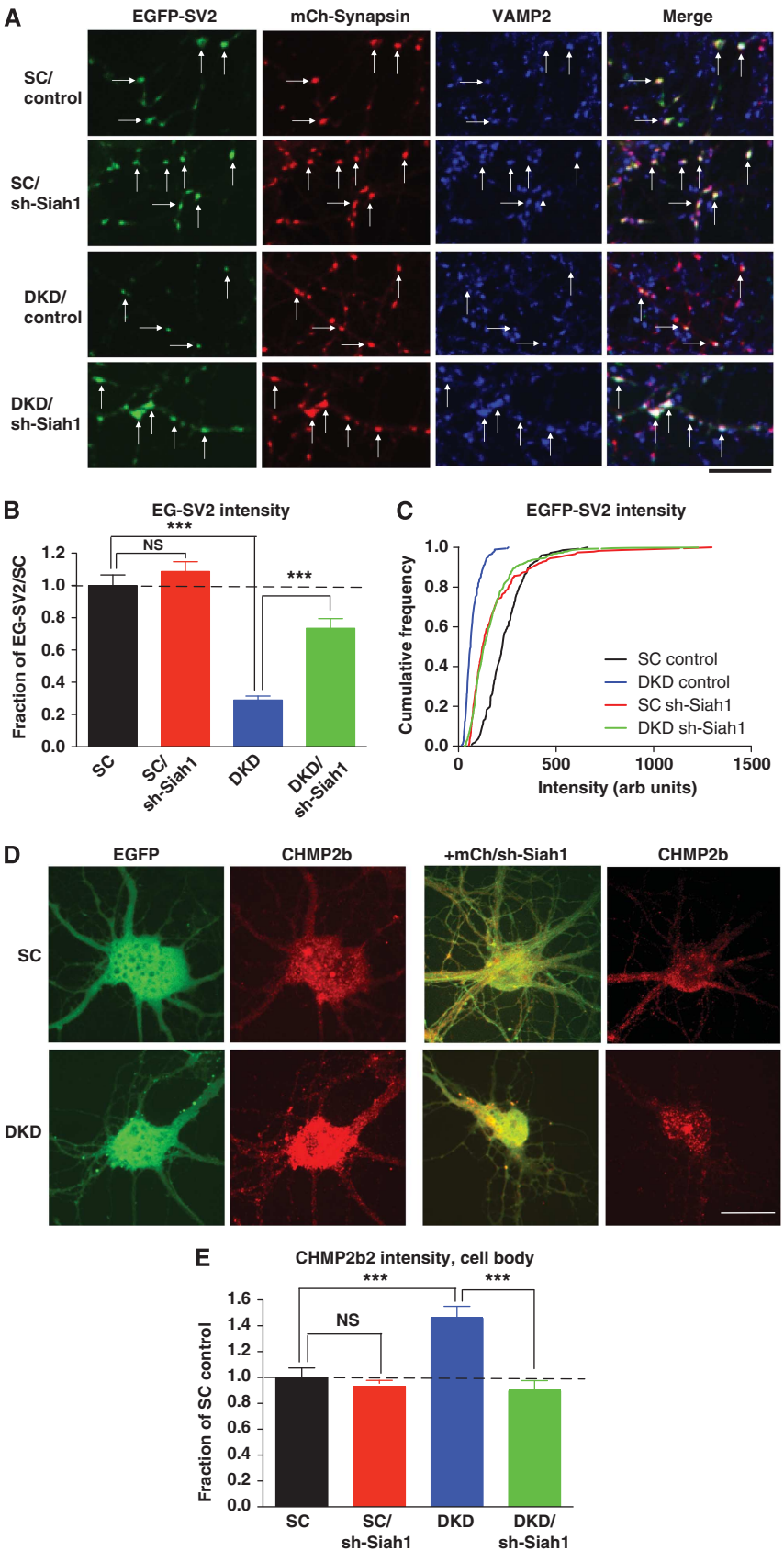

Siah1 expression is inversely related to SV pool size

If Bassoon and Piccolo negatively regulate Siah1's activity, then another prediction is that Siah1 knockdown should ameliorate DKD phenotypes such as presynaptic protein loss and increased endo-lysosomal organelle expression. To test this hypothesis, we designed an shRNA that effectively downregulated Siah1 (sh-Siah1; Supplementary Figure S6), and subcloned it into the lentiviral vector together with mCherry-Synapsin1a (mCh-Syn) to label presynaptic boutons. Neurons co-transduced with EGFP-SV2/SC or EGFP-SV2/DKD and mCh-Syn ± sh-Siah1 at the time of plating were fixed and assessed for EGFP-SV2 fluorescence intensity at 14 DIV. Expression of mCh-Syn alone did not significantly alter EGFP-SV2 fluorescence in control or DKD boutons, indicating that Synapsin overexpression neither altered SV pool size nor rescued the DKD phenotype (Figure 9A). Similarly, sh-Siah1 expression did not change EGFP-SV2 levels in control boutons (Figure 9A–C). In contrast, DKD boutons expressing mCh-Syn/sh-Siah1 had significantly increased (by $>40\%$) EGFP-SV2 fluorescence intensities (Figure 9A–C), demonstrating that Siah1 knockdown partially rescued the DKD phenotype. These data further support the concept that Siah1 activity contributes to SV loss seen at Bassoon/Piccolo-deficient boutons.

To asses whether Siah1 knockdown similarly mitigated DKD-induced upregulation of endo-lysosomal organelles, we examined CHMP2b immunofluorescence in cell bodies of neurons cotransduced with EGFP/SC or/DKD and mCherry/sh-Siah1. Interestingly, co-expression of mCherry/sh-Siah1 significantly reduced CHMP2b intensity in DKD cell bodies, normalizing its levels to those seen in SC neurons (Figure 9D and E). In contrast, no significant changes in CHMP2b fluorescence were observed in SC neurons expressing mCherry/sh-Siah1 (Figure 9D and E). These findings further demonstrate that Siah1-mediated ubiquitination promotes the aberrant degradation of presynaptic proteins and concomitant upregulation of endo-lysosomal machinery in neurons lacking Bassoon and Piccolo.

Discussion

Our results demonstrate a novel and unexpected role for Bassoon and Piccolo in maintaining protein homeostasis within presynaptic boutons. Specifically, we find that knockdown of these highly homologous AZ proteins promotes the ubiquitination and degradation of multiple presynaptic proteins, resulting in synapse degeneration. An important component of this degradative pathway is the E3 ligase Siah1, whose activity is negatively regulated by the ZF domains of Bassoon and Piccolo. These findings implicate Bassoon and Piccolo as important regulators of protein ubiquitination within the presynaptic AZ.

Bassoon and Piccolo as regulators of SV stasis

An important aspect of presynaptic proteostasis is the maintenance of SV pools (SV stasis) within boutons. Such pools are necessary to support the sustained release of neurotransmitter by maintaining a local reservoir of SV-associated proteins and membranes to facilitate vesicle recycling (Denker *et al*, 2011a, b). Several lines of evidence support a role for Bassoon and Piccolo in SV stasis. First, their double knockdown causes a dramatic loss of SV-associated proteins, including synaptophysin, VAMP2, SV2, and synapsin1a, as assessed by immunoblotting, immunofluorescence microscopy, and expression of recombinant-tagged proteins. Second, EM analysis of DKD boutons reveals significant abnormalities in SV abundance and morphology, including decreased SVs/bouton, increased numbers of elongated and enlarged SVs, and the appearance of numerous pleiomorphic vesicles reminiscent of endo-lysosomal structures. Between 9 and 14 DIV, these structures increase dramatically in prevalence while SVs disappear, suggesting that they represent intermediates in a pathway for SV degradation. Moreover, using markers to visualize lysosomes and MVBs (LysoTracker and CHMP2b, respectively), we find that these organelles are significantly upregulated in DKD neurons. Lysosomes in particular appear concentrated in the axon initial segment, a position that would facilitate the degradation of retrogradely transported SV-derived membranes and proteins. Finally, genetic and pharmacological manipulations that inhibit protein ubiquitination and degradation mitigate DKD-induced loss of SV-associated proteins. These findings indicate that Bassoon and Piccolo are critically important for maintaining SV pools within presynaptic boutons.

Although less robust, a similar phenotype of SV loss was observed by Mukherjee *et al* (2010) in their recent study of Bassoon/Piccolo-deficient neurons. These authors performed an ultrastructural analysis of neurons cultured from $Pclo^{\Delta exon14}$ mice and infected with an shRNA to knockdown Bassoon expression. They found an $\sim 50\%$ reduction in both total and docked SVs/bouton with no other morphological defects, leading the authors to conclude that Bassoon and Piccolo have a role in SV clustering. However, these findings

Figure 9 Siah1 knockdown mitigates DKD-induced protein degradation. (**A**) Fourteen DIV neurons co-expressing EGFP-SV2/SC or/DKD together with mCh-Synapsin ± shRNAs to knockdown Siah1 (sh-Siah1), immunostained with VAMP2. Arrows indicate boutons that express both green and red constructs. Siah1 knockdown increases both EGFP-SV2 and VAMP2 fluorescence in the DKD background. Brightness of mCh-Synapsin has been standardized across conditions to illustrate its colocalization with EGFP-SV2, and does not reflect actual intensity. Size bar is 10 μm. (**B**) EGFP-SV2 intensity ± sh-Siah1. Values are expressed as fraction of EGFP-SV2 intensity at SC boutons co-expressing mCh-Synapsin (dashed line). Siah1 knockdown increases EGFP-SV2 fluorescence at DKD boutons by $\sim 45\%$, but has no significant effect in SC control boutons ($n \geqslant 4$ fields of view/condition, >30 puncta/field; $^{***}P<0.0005$, unpaired *t*-test). (**C**) Cumulative frequency distribution of EGFP-SV2 fluorescence intensity in SC and DKD boutons expressing sh-Siah1. Siah1 knockdown partially prevents DKD-induced loss of boutons, shifting the EGFP-SV2 intensity distribution to the right. Values are from (**B**) ($n = 147$ SC + mCh-Syn, 187 DKD + mCh-Syn, 248 SC + mCh-Syn/shSiah1, 495 DKD + mCh-Syn/shSiah1 boutons). (**D**) Left two panels: 14 DIV neurons transduced with EGFP/SC or/DKD at the time of plating and immunostained with CHMP2b. CHMP2b fluorescence is enhanced in the DKD cell body. Right two panels: 14 DIV neurons co-transduced with EGFP/SC or/DKD and mCherry/sh-Siah1 (merged fluorescence is shown). Siah1 knockdown normalizes CHMP2b immunofluorescence in the DKD background. Size bar is 20 μm. (**E**) CHMP2b immunofluorescence intensity, expressed as fraction of average fluorescence intensity in SC cell bodies (dashed line). DKD neurons exhibit 50% more CHMP2b fluorescence than SC neurons, and this phenotype is normalized by Siah1 knockdown. Data for SC and DKD controls are from Figure 5D ($n \geqslant 15$ cells/condition, three independent experiments; $^{***}P<0.0001$).

likely reflect a weak version of the DKD phenotype caused by incomplete knockdown of both proteins. This conclusion is supported by the authors' own experiments demonstrating that only ~70% of Bassoon was eliminated by shRNA knockdown (Mukherjee *et al*, 2010). Moreover, our analysis of $Pclo^{\Delta exon14}$ mice revealed that only three of the seven identified Piccolo isoforms were eliminated, and that the remaining isoforms, all of which contain the ZFs, localize to presynaptic boutons. Importantly, we also found that Piccolo loss-of-function phenotypes were not present in neurons cultured from $Pclo^{\Delta exon14}$ mice, unless remaining isoforms were eliminated by shRNA knockdown (Waites *et al*, 2011). Thus, we believe that the ultrastructural data from the study by Mukherjee and colleagues are consistent with ours, demonstrating a role for Piccolo and Bassoon in regulating SV pool maintenance and not just SV clustering.

Modulation of Siah1 activity by Bassoon and Piccolo ZFs

An important molecule in Piccolo/Bassoon-dependent proteostasis is the E3 ubiquitin ligase Siah1. Siah1 was initially identified as a Bassoon interacting partner in a yeast two-hybrid screen, and is particularly fascinating in the context of presynaptic protein ubiquitination/degradation, as its substrates include multiple SV-associated proteins (Liu *et al*, 2001; Wheeler *et al*, 2002; Liani *et al*, 2004; Szargel *et al*, 2009; Dimitrova *et al*, 2010). Co-immunoprecipitation assays confirm that the Siah1-Bassoon interaction depends upon the RING domain of Siah1 and the N-terminal ZF domains of Bassoon. The former domain also interacts with E2 ubiquitin conjugating enzymes to facilitate protein ubiquitination, while the latter contains two ZFs that are highly homologous to a pair of ZFs in the N-terminus of Piccolo (Fenster *et al*, 2000). This homology provides a potential explanation for why SV loss and synapse degeneration is only observed in neurons lacking both Bassoon and Piccolo, and thus all four ZFs (Altrock *et al*, 2003; Leal-Ortiz *et al*, 2008). This concept is further supported by the capacity of each ZF to suppress the loss of EGFP-SV2 fluorescence in DKD boutons.

Importantly, we also find that Siah1 is necessary for regulating presynaptic proteostasis in a Piccolo/Bassoon-dependent manner. For example, Siah1 knockdown in the DKD background restores EGFP-SV2 fluorescence to near wild-type levels, and simultaneously attenuates the upregulation of MVBs. Moreover, overexpression of EGFP-Siah1 in wild-type neurons dramatically reduces both the number of presynaptic boutons/unit length of axon and the size of remaining boutons (Supplementary Figure S6). Together, these data indicate that the Bassoon/Piccolo ZFs maintain synapse integrity in part by negatively regulating Siah1's ubiquitin ligase activity within presynaptic boutons. Since Siah1 knockdown does not completely rescue SV loss, and the ZFs are predicted to interact with other RING domains, it is very likely that additional E3 ligases also mediate the DKD phenotypes. Furthermore, since both proteasomal and lysosomal degradation are increased in DKD neurons, and KO ubiquitin does not completely rescue the DKD phenotypes, it is probable that non-ubiquitin-based degradative pathways such as macroautophagy also contribute to protein loss in the absence of Bassoon and Piccolo. Additional experiments are needed to investigate this hypothesis.

Ubiquitination and neurodegeneration

An emerging theme from this and other studies is that alterations in protein ubiquitination at the synapse can trigger neurodegeneration (Almeida *et al*, 2006; Chou *et al*, 2008; Ding and Shen, 2008; Engelender, 2008; Lehman, 2009). Genetic KO of several enzymes that regulate ubiquitination, including the E3 ligase Scrapper and the deubiquitinating enzymes UCH-L1 and Usp14, cause abnormal SV morphology/density within boutons, synapse degeneration, and premature death of the organism due to central or peripheral nervous system degeneration (Yao *et al*, 2008; Chen *et al*, 2009, 2010). Bassoon/Piccolo DKD also leads to abnormal bouton and SV morphology, upregulation of endo-lysosomal organelles, and progressive degeneration of synapses. Since these phenotypes emerge concomitantly with Bassoon/Piccolo loss, it seems likely that DKD-induced changes in protein ubiquitination originate at or near the presynaptic AZ. Moreover, the phenotypic parallels between Bassoon/Piccolo DKD and these other genetic manipulations suggest that the DKD will also adversely impact neuronal health over time. Future studies will explore this issue.

Although presynaptic degeneration is the dominant phenotype observed in DKD boutons, it is currently unclear whether maintaining presynaptic proteostasis is a primary function of Bassoon and Piccolo, or whether this phenotype is simply a consequence of aberrant local protein ubiquitination/degradation, similar to what may occur in neurodegenerative disorders such as Parkinson's, Huntington's, and Alzheimer's diseases. As core components of the CAZ, Bassoon and Piccolo may normally regulate the local ubiquitination of presynaptic proteins and receptors as they dynamically transit into and out of the AZ plasma membrane. A number of emerging studies suggest that such a role would be instrumental for proper synaptic function, given the importance of ubiquitination in neurotransmitter release, presynaptic plasticity, and neurotrophin retrograde signalling (Hicke, 2001; Hicke and Dunn, 2003; DiAntonio and Hicke, 2004; Geetha and Wooten, 2008; Jiang *et al*, 2010; Rinetti and Schweizer, 2010). Future studies will investigate the role of the Bassoon/Piccolo/Siah1 interaction in these processes.

Materials and methods

Reagents

Please see Supplementary data for a complete list of reagents and vendors.

Design of DNA constructs

DKD lentiviral vectors. shRNAs against Piccolo and Bassoon were described previously (Leal-Ortiz *et al*, 2008). Design of the tricistronic lentiviral vector is described in Supplementary data.

shRNA-resistant Bassoon. RFP-tagged shRNA-resistant Bassoon (Bsn*) was created from RFP 95-3938 Bassoon (NM_019146) using double PCR to introduce a point mutation (see Supplementary data for details of this procedure). The RFP-Bsn* cassette, together with Pclo28 and Bsn16 shRNAs, was then subcloned into the helper-dependent adenoviral vector (Palmer and Ng, 2011).

mCherry-tagged Bsn and Pclo ZFs. ZFs were amplified from full-length Bassoon (rat) and an N-terminal, 4.1 kb fragment of Piccolo (rat) using a series of primers (see Supplementary data). PCR products were subcloned into mCherry-N2 vector at the *Hin*dIII and *Bgl*II sites, sequenced, then subcloned into FUGW vector at the *Xba*1/*Eco*R1 sites for lentiviral expression.

Siah1 constructs and shRNAs, mCherry-1D2A-HA-ubiquitin KO vector. See Supplementary data for the design of these constructs.

Helper-dependent adenovirus production

Helper-dependent adenovirus (HDAd) was produced as previously described (Palmer and Ng, 2011). Neurons expressing EGFP-SV2/SC and/DKD were transduced with RFP-Bsn* adenovirus at 5 DIV.

Hippocampal culture, lentiviral infection, and electroporation

Primary hippocampal cultures were prepared using a modified Banker culture protocol, as previously described (Waites *et al*, 2009). Neurons were transduced with lentivirus on 0–1 DIV, as described (Leal-Ortiz *et al*, 2008; Waites *et al*, 2009). Several plasmids were introduced by electroporation into 0 DIV hippocampal neurons prior to plating. VAMP2-HRP was electroporated using the Amaxa/Lonza nucleofector, according to manufacturer's protocol (Lonza). EGFP-SV2 constructs were electroporated using standard methods (see Supplementary data).

Western/immunoblot analysis

Cellular lysates from lentivirally transduced hippocampal neurons were collected in reducing sample buffer (Bio-Rad), separated by SDS–PAGE, transferred onto nitrocellulose membranes, and immunoblotted in 5% BSA/PBST (PBS with 0.05% Tween-20) with the primary antibodies described above followed by DyLight 680 and 800 anti-mouse and anti-rabbit secondary antibodies (Thermo Scientific/Pierce). Blots were imaged using the Odyssey Infrared Imager (Model 9120, LI-COR Biosciences). Protein immunoreactivity was measured and normalized to tubulin levels using the gel analysis module in ImageJ.

Light and electron microscopy

Immunofluorescence microscopy. Neurons were fixed and processed for immunofluorescence as previously described (Leal-Ortiz *et al*, 2008), using a series of primary antibodies (see above). Alexa-568 and 647 (anti-mouse and anti-rabbit, highly adsorbed; Invitrogen) were used as secondary antibodies. Images were acquired on a spinning disc confocal microscope (Zeiss Axiovert 200M with Perkin-Elmer spinning disc and Melles Griot 43 series Ion laser), using a $\times 63$ Plan-Apochromat objective (NA 1.4), photometrics Cascade 512B digital camera (Roper Scientific) and MetaMorph software (Molecular Devices).

Quantification of puncta intensity. Intensity of EGFP-SV2 or immunolabelled puncta of synaptic proteins (i.e., synaptophysin, VAMP2) was measured using OpenView software (written by Dr Noam Ziv, Technion Institute, Haifa, Israel) and resulting values analysed/normalized in Excel. Graphing and statistics were performed in Prism (GraphPad). See Supplementary data for a detailed explanation of our puncta intensity analysis method.

LysoTracker imaging and quantification. Neurons were incubated in 75 nM LysoTracker Red in normal Tyrode's solution for 45 min at 37°C. Images of neuronal cell bodies were acquired as Z-stacks on the spinning disc confocal microscope (described above). Image analysis (to count number of LysoTracker puncta/cell) was performed in ImageJ. See Supplementary data for a detailed explanation of this analysis.

Quantification of CHMP2b fluorescence intensity. The fluorescence intensity of CHMP2b immunostaining within EGFP/SC and EGFP/DKD cell bodies and axons was measured using ImageJ. See Supplementary data for a more detailed explanation of this procedure.

Image processing. Representative images shown in figures depict regions of interest (ROIs) selected from the original images. ROIs selected from images acquired on the spinning disc confocal microscope are typically 140×75 pixels (from the full-sized 512×512 pixel image). In addition, brightness/contrast is often enhanced to enable easier visualization of EGFP-Synapsin, EGFP-SV2, and other presynaptic markers. Therefore, the original image resolution and full dynamic range of fluorescence intensity are not always apparent from the images shown.

Electron microscopy. Cultured hippocampal neurons electroporated with VAMP-HRP/SC or/DKD were processed for EM on 9 or 14 DIV as previously described (Leal-Ortiz *et al*, 2008). See Supplementary data for detailed explanations of EM micrograph quantification procedures.

Immunoprecipitation assays

Immunoprecipitation of proteins from synaptosomes. Crude synaptosomes were prepared as described in Lopez-Perez (1994)), but scaled down for smaller volume. See Supplementary data for a more detailed description of this procedure. VAMP2 and synaptophysin were subsequently immunoprecipitated using the described antibodies (Supplementary data) conjugated to Dynabeads (Invitrogen). Bound material was eluted from beads into sample buffer, and immunoblotted as described above.

Co-immunoprecipitation. Co-IPs with myc-Siah1 and mCh-ZFs co-transfected into HEK cells were performed using a myc immunoprecipitation kit (Pierce/Thermo Scientific), according to manufacturer's instructions. See Supplementary data for details.

Supplementary data

Supplementary data are available at *The EMBO Journal* Online (http://www.embojournal.org).

Acknowledgements

We would like to thank Zhaolin Hua and Rob Edwards (UCSF) for assistance with Amaxa/Lonza electroporation; Phillip Ng (Baylor College of Medicine) for graciously providing helper-dependent, non-replicating adenovirus; Ted Dawson for the original pRK5-Ubiquitin-KO plasmid (Addgene plasmid 17603); members of the Garner and Waites laboratories for their scientific input, and Noam Ziv (Technion Institute, Israel) for generously providing and offering assistance with OpenView image analysis software. This work was supported by NIH grants NS39471 and NS353862 and United States/Israel Binational Science Foundation (2007425) to CCG and Columbia University Departments of Pathology and Cell Biology and Neuroscience startup funds to CLW. AF was supported by DFG FE-1335/1.

Author contributions: CW conceived of and designed experiments, acquired/analysed data, supervised data acquisition, wrote manuscript. SL-O conceived of and designed experiments, acquired/analysed data. NO acquired/analysed data. HD acquired/analysed data. AF acquired/analysed data. WA acquired/analysed data. EG supervised data acquisition. CG conceived of and designed experiments, supervised data acquisition, wrote manuscript.

Conflict of interest

The authors declare that they have no conflict of interest.

References

Almeida CG, Takahashi RH, Gouras GK (2006) Beta-amyloid accumulation impairs multivesicular body sorting by inhibiting the ubiquitin-proteasome system. *J Neurosci* **26:** 4277–4288

Altick AL, Baryshnikova LM, Vu TQ, von Bartheld CS (2009) Quantitative analysis of multivesicular bodies (MVBs) in the hypoglossal nerve: evidence that neurotrophic factors do not use MVBs for retrograde axonal transport. *J Comp Neurol* **514:** 641–657

Altrock WD, tom Dieck S, Sokolov M, Meyer AC, Sigler A, Brakebusch C, Fassler R, Richter K, Boeckers TM, Potschka H, Brandt C, Löscher W, Grimberg D, Dresbach T, Hempelmann A, Hassan H, Balschun D, Frey JU, Brandstätter JH, Garner CC *et al* (2003) Functional inactivation of a fraction of excitatory synapses

in mice deficient for the active zone protein bassoon. *Neuron* **37:** 787–800

Bajjalieh SM, Frantz GD, Weimann JM, McConnell SK, Scheller RH (1994) Differential expression of synaptic vesicle protein 2 (SV2) isoforms. *J Neurosci* **14:** 5223–5235

Cases-Langhoff C, Voss B, Garner AM, Appeltauer U, Takei K, Kindler S, Veh RW, De Camilli P, Gundelfinger ED, Garner CC (1996) Piccolo, a novel 420 kDa protein associated with the presynaptic cytomatrix. *Eur J Cell Biol* **69:** 214–223

Chen F, Sugiura Y, Myers KG, Liu Y, Lin W (2010) Ubiquitin carboxyl-terminal hydrolase L1 is required for maintaining the structure and function of the neuromuscular junction. *Proc Natl Acad Sci USA* **107:** 1636–1641

Chen PC, Qin LN, Li XM, Walters BJ, Wilson JA, Mei L, Wilson SM (2009) The proteasome-associated deubiquitinating enzyme Usp14 is essential for the maintenance of synaptic ubiquitin levels and the development of neuromuscular junctions. *J Neurosci* **29:** 10909–10919

Chou AP, Maidment N, Klintenberg R, Casida JE, Li S, Fitzmaurice AG, Fernagut PO, Mortazavi F, Chesselet MF, Bronstein JM (2008) Ziram causes dopaminergic cell damage by inhibiting E1 ligase of the proteasome. *J Biol Chem* **283:** 34696–34703

Denker A, Bethani I, Krohnert K, Korber C, Horstmann H, Wilhelm BG, Barysch SV, Kuner T, Neher E, Rizzoli SO (2011a) A small pool of vesicles maintains synaptic activity *in vivo*. *Proc Natl Acad Sci USA* **108:** 17177–17182

Denker A, Krohnert K, Buckers J, Neher E, Rizzoli SO (2011b) The reserve pool of synaptic vesicles acts as a buffer for proteins involved in synaptic vesicle recycling. *Proc Natl Acad Sci USA* **108:** 17183–17188

DiAntonio A, Hicke L (2004) Ubiquitin-dependent regulation of the synapse. *Annu Rev Neurosci* **27:** 223–246

Dick O, tom Dieck S, Altrock WD, Ammermuller J, Weiler R, Garner CC, Gundelfinger ED, Brandstatter JH (2003) The presynaptic active zone protein bassoon is essential for photoreceptor ribbon synapse formation in the retina. *Neuron* **37:** 775–786

Dimitrova YN, Li J, Lee YT, Rios-Esteves J, Friedman DB, Choi HJ, Weis WI, Wang CY, Chazin WJ (2010) Direct ubiquitination of beta-catenin by Siah-1 and regulation by the exchange factor TBL1. *J Biol Chem* **285:** 13507–13516

Ding M, Shen K (2008) The role of the ubiquitin proteasome system in synapse remodeling and neurodegenerative diseases. *Bioessays* **30:** 1075–1083

Ehlers MD (2003) Activity level controls postsynaptic composition and signaling via the ubiquitin-proteasome system. *Nat Neurosci* **6:** 231–242

Engelender S (2008) Ubiquitination of alpha-synuclein and autophagy in Parkinson's disease. *Autophagy* **4:** 372–374

Fejtova A, Gundelfinger ED (2006) Molecular organization and assembly of the presynaptic active zone of neurotransmitter release. *Results Probl Cell Differ* **43:** 49–68

Fenster SD, Chung WJ, Zhai R, Cases-Langhoff C, Voss B, Garner AM, Kaempf U, Kindler S, Gundelfinger ED, Garner CC (2000) Piccolo, a presynaptic zinc finger protein structurally related to bassoon. *Neuron* **25:** 203–214

Frank T, Rutherford MA, Strenzke N, Neef A, Pangrsic T, Khimich D, Fejtova A, Gundelfinger ED, Liberman MC, Harke B, Bryan KE, Lee A, Egner A, Riedel D, Moser T (2010) Bassoon and the synaptic ribbon organize Ca(2) + channels and vesicles to add release sites and promote refilling. *Neuron* **68:** 724–738

Friedman HV, Bresler T, Garner CC, Ziv NE (2000) Assembly of new individual excitatory synapses: time course and temporal order of synaptic molecule recruitment. *Neuron* **27:** 57–69

Geetha T, Wooten MW (2008) TrkA receptor endolysosomal degradation is both ubiquitin and proteasome dependent. *Traffic* **9:** 1146–1156

Hallermann S, Fejtova A, Schmidt H, Weyhersmuller A, Silver RA, Gundelfinger ED, Eilers J (2010) Bassoon speeds vesicle reloading at a central excitatory synapse. *Neuron* **68:** 710–723

Harlow ML, Ress D, Stoschek A, Marshall RM, McMahan UJ (2001) The architecture of active zone material at the frog's neuromuscular junction. *Nature* **409:** 479–484

Hicke L (2001) Protein regulation by monoubiquitin. *Nat Rev Mol Cell Biol* **2:** 195–201

Hicke L, Dunn R (2003) Regulation of membrane protein transport by ubiquitin and ubiquitin-binding proteins. *Annu Rev Cell Dev Biol* **19:** 141–172

Hua Z, Leal-Ortiz S, Foss SM, Waites CL, Garner CC, Voglmaier SM, Edwards RH (2011) v-SNARE composition distinguishes synaptic vesicle pools. *Neuron* **71:** 474–487

Jiang X, Litkowski PE, Taylor AA, Lin Y, Snider BJ, Moulder KL (2010) A role for the ubiquitin-proteasome system in activity-dependent presynaptic silencing. *J Neurosci* **30:** 1798–1809

Jin Y, Garner CC (2008) Molecular mechanisms of presynaptic differentiation. *Annu Rev Cell Dev Biol* **24:** 237–262

Leal-Ortiz S, Waites CL, Terry-Lorenzo R, Zamorano P, Gundelfinger ED, Garner CC (2008) Piccolo modulation of Synapsin1a dynamics regulates synaptic vesicle exocytosis. *J Cell Biol* **181:** 831–846

Lee CS, Tee LY, Warmke T, Vinjamoori A, Cai A, Fagan AM, Snider BJ (2004) A proteasomal stress response: pre-treatment with proteasome inhibitors increases proteasome activity and reduces neuronal vulnerability to oxidative injury. *J Neurochem* **91:** 996–1006

Lee S, Sato Y, Nixon RA (2011) Lysosomal proteolysis inhibition selectively disrupts axonal transport of degradative organelles and causes an Alzheimer's-like axonal dystrophy. *J Neurosci* **31:** 7817–7830

Lehman NL (2009) The ubiquitin proteasome system in neuropathology. *Acta Neuropathol* **118:** 329–347

Liani E, Eyal A, Avraham E, Shemer R, Szargel R, Berg D, Bornemann A, Riess O, Ross CA, Rott R, Engelender S (2004) Ubiquitylation of synphilin-1 and alpha-synuclein by SIAH and its presence in cellular inclusions and Lewy bodies imply a role in Parkinson's disease. *Proc Natl Acad Sci USA* **101:** 5500–5505

Lim KL, Chew KC, Tan JM, Wang C, Chung KK, Zhang Y, Tanaka Y, Smith W, Engelender S, Ross CA, Dawson VL, Dawson TM (2005) Parkin mediates nonclassical, proteasomal-independent ubiquitination of synphilin-1: implications for Lewy body formation. *J Neurosci* **25:** 2002–2009

Liu J, Stevens J, Rote CA, Yost HJ, Hu Y, Neufeld KL, White RL, Matsunami N (2001) Siah-1 mediates a novel beta-catenin degradation pathway linking p53 to the adenomatous polyposis coli protein. *Mol Cell* **7:** 927–936

Lopez-Perez MJ (1994) Preparation of synaptosomes and mitochondria from mammalian brain. *Methods Enzymol* **228:** 403–411

Moriyoshi K, Iijima K, Fujii H, Ito H, Cho Y, Nakanishi S (2004) Seven in absentia homolog 1A mediates ubiquitination and degradation of group 1 metabotropic glutamate receptors. *Proc Natl Acad Sci USA* **101:** 8614–8619

Mukherjee K, Yang X, Gerber SH, Kwon HB, Ho A, Castillo PE, Liu X, Sudhof TC (2010) Piccolo and bassoon maintain synaptic vesicle clustering without directly participating in vesicle exocytosis. *Proc Natl Acad Sci USA* **107:** 6504–6509

Palmer DJ, Ng P (2011) Rescue, amplification, and large-scale production of helper-dependent adenoviral vectors. *Cold Spring Harb Protoc* **2011:** 857–866

Parton RG, Simons K, Dotti CG (1992) Axonal and dendritic endocytic pathways in cultured neurons. *J Cell Biol* **119:** 123–137

Rinetti GV, Schweizer FE (2010) Ubiquitination acutely regulates presynaptic neurotransmitter release in mammalian neurons. *J Neurosci* **30:** 3157–3166

Santelli E, Leone M, Li C, Fukushima T, Preece NE, Olson AJ, Ely KR, Reed JC, Pellecchia M, Liddington RC, Matsuzawa S (2005) Structural analysis of Siah1-Siah-interacting protein interactions and insights into the assembly of an E3 ligase multiprotein complex. *J Biol Chem* **280:** 34278–34287

Schoch S, Gundelfinger ED (2006) Molecular organization of the presynaptic active zone. *Cell Tissue Res* **326:** 379–391

Shapira M, Zhai RG, Dresbach T, Bresler T, Torres VI, Gundelfinger ED, Ziv NE, Garner CC (2003) Unitary assembly of presynaptic active zones from Piccolo-Bassoon transport vesicles. *Neuron* **38:** 237–252

Siksou L, Rostaing P, Lechaire JP, Boudier T, Ohtsuka T, Fejtova A, Kao HT, Greengard P, Gundelfinger ED, Triller A, Marty S (2007) Three-dimensional architecture of presynaptic terminal cytomatrix. *J Neurosci* **27:** 6868–6877

Szargel R, Rott R, Eyal A, Haskin J, Shani V, Balan L, Wolosker H, Engelender S (2009) Synphilin-1A inhibits seven in absentia homolog (SIAH) and modulates alpha-synuclein monoubiquitylation and inclusion formation. *J Biol Chem* **284:** 11706–11716

tom Dieck S, Altrock WD, Kessels MM, Qualmann B, Regus H, Brauner D, Fejtova A, Bracko O, Gundelfinger ED, Brandstatter JH (2005) Molecular dissection of the photoreceptor ribbon synapse: physical interaction of Bassoon and RIBEYE is essential for the assembly of the ribbon complex. *J Cell Biol* **168:** 825–836

Varshavsky A (2005) Regulated protein degradation. *Trends Biochem Sci* **30:** 283–286

Waites CL, Craig AM, Garner CC (2005) Mechanisms of vertebrate synaptogenesis. *Annu Rev Neurosci* **28:** 251–274

Waites CL, Garner CC (2011) Presynaptic function in health and disease. *Trends Neurosci* **34:** 326–337

Waites CL, Leal-Ortiz SA, Andlauer TF, Sigrist SJ, Garner CC (2011) Piccolo regulates the dynamic assembly of presynaptic F-actin. *J Neurosci* **31:** 14250–14263

Waites CL, Specht CG, Hartel K, Leal-Ortiz S, Genoux D, Li D, Drisdel RC, Jeyifous O, Cheyne JE, Green WN, Montgomery JM, Garner CC (2009) Synaptic SAP97 isoforms regulate AMPA receptor dynamics and access to presynaptic glutamate. *J Neurosci* **29:** 4332–4345

Wheeler TC, Chin LS, Li Y, Roudabush FL, Li L (2002) Regulation of synaptophysin degradation by mammalian homologues of seven in absentia. *J Biol Chem* **277:** 10273–10282

Willeumier K, Pulst SM, Schweizer FE (2006) Proteasome inhibition triggers activity-dependent increase in the size of the recycling vesicle pool in cultured hippocampal neurons. *J Neurosci* **26:** 11333–11341

Yao I, Sugiura Y, Matsumoto M, Setou M (2008) *In situ* proteomics with imaging mass spectrometry and principal component analysis in the Scrapper-knockout mouse brain. *Proteomics* **8:** 3692–3701

Yi JJ, Ehlers MD (2005) Ubiquitin and protein turnover in synapse function. *Neuron* **47:** 629–632

Zhai R, Olias G, Chung WJ, Lester RA, tom Dieck S, Langnaese K, Kreutz MR, Kindler S, Gundelfinger ED, Garner CC (2000) Temporal appearance of the presynaptic cytomatrix protein bassoon during synaptogenesis. *Mol Cell Neurosci* **15:** 417–428

Ziv NE, Garner CC (2004) Cellular and molecular mechanisms of presynaptic assembly. *Nat Rev Neurosci* **5:** 385–399